frontiers | Frontiers in Chemical Biology

TYPE Original Research
PUBLISHED 03 February 2025
DOI 10.3389/fchbi.2025.1547323

OPEN ACCESS

EDITED BY
Richard C. Holz,
Colorado School of Mines, United States

REVIEWED BY
Joanna Burger,
Wroclaw Medical University, Poland
Theodore Holman,
University of California, Santa Cruz,
United States

*CORRESPONDENCE
Aviva Levina,
aviva.levina@sydney.edu.au
Debbie C. Crans,
debbie.crans@colostate.edu
Peter A. Lay,
peter.lay@sydney.edu.au

RECEIVED 18 December 2024
ACCEPTED 14 January 2025
PUBLISHED 03 February 2025

CITATION
Levina A, Crans DC and Lay PA (2025) Reactivity in cell culture medium and *in vitro* anticancer activity of 3,5-di-*tert*-butylcatechol: link to metal-catechol interactions.
Front. Chem. Biol. 4:1547323.
doi: 10.3389/fchbi.2025.1547323

Reactivity in cell culture medium and *in vitro* anticancer activity of 3,5-di-*tert*-butylcatechol: link to metal-catechol interactions

Aviva Levina[1]*, Debbie C. Crans[2]* and Peter A. Lay[1]*

[1]School of Chemistry, The University of Sydney, Sydney, NSW, Australia, [2]Department of Chemistry and Cell and Molecular Biology Program, Colorado State University, Fort Collins, CO, United States

Introduction: Catechol moieties are common in natural bioactive molecules, and their ability to bind metal ions is widely explored both naturally with siderophores and in the development of metal-based drugs. The reactivities and biology activities of a sterically hindered model catechol compound, 3,5-di-*tert*-butylcatechol ($dtbH_2$) and its oxidation product 3,5-di-*tert*-butyl-*o*-quinone (dtbQ), were studied in cell culture medium to understand better the medicinal roles of this class of molecules.

Methods: Anti-proliferative activities of $dtbH_2$ and dtbQ in fresh and aged solutions of the molecules were studied in two common human cancer cell lines, T98G (glioblastoma) and A549 (lung carcinoma). Electrospray mass spectrometry and UV/Vis spectroscopy were used to study the reactivities of the molecules in buffer solutions and cell culture medium, in the presence and absence of glutathione and imidazole.

Results and Discussion: The $dtbH_2$ and dtbQ molecules showed high anti-proliferative activity (IC_{50} < 10 μM in 72 h assays) in T98G and A549 cell lines in the absence of added metal ions. The activity was observed when $dtbH_2$ and dtbQ were freshly added to cell culture medium, while pre-incubation with the medium for 24 h reduced their activity 5-10-fold. This deactivation was avoided when the biological reductant, glutathione (GSH), was added to the medium at a physiologically relevant intracellular concentration (5.0 mM). These results were explained by speciation studies (UV/Vis spectroscopy and mass spectrometry) of $dtbH_2$ and dtbQ in cell culture medium, aqueous buffers, or organic solvents in the presence or absence of GSH. These studies showed that a redox equilibrium was established between $dtbH_2$ and dtbQ, with the latter rapidly coupling the GSH in an oxidative manner. The resultant adduct is likely to be responsible for the high toxicity of $dtbH_2$ and dtbQ in GSH-rich cancer cells via oxygen-dependent radical chain reactions. Deactivation of $dtbH_2$ and dtbQ in cell culture medium in the absence of GSH was due to the reactions of dtbQ with nucleophiles, such as amino acids, followed by the formation of polymeric species. The reported high anti-proliferative activity of V(V)-catecholato complexes can be explained by a combination of their efficient cellular uptake and rapid decomposition in thiol-rich intracellular environment with the formation of active V(V) and $dtbH_2$/dtbQ adducts with thiols (mainly GSH). Slower decomposition and deactivation of the

complexes was observed in thiol-poor extracellular environments. These data show that speciation in cell culture medium is crucial for the biological activity not only of metal complexes but also of their ligands when the complexes dissociates.

KEYWORDS

catechol, quinone, vanadium, glutathione, cell culture medium, reactive oxygen species, anti-proliferative assays, catechol-glutathione adduct

1 Introduction

The crucial role of speciation in biological media, including cell culture media (CCM), in the mechanism of action of most biologically active transition metal complexes is now well established (Levina et al., 2017; Stone et al., 2021; Hall, 2022; Dinda et al., 2025). The abundance of ligands for metal ions, such as amino acids, in CCM, can lead to substitution reactions of metal complexes and the release of free ligands, which are often the main species responsible for the biological activity (Levina and Lay, 2017; Reytman et al., 2018; Nunes et al., 2021; Levina et al., 2024). It is less well known that the ligands released in such reactions can undergo further chemical changes in CCM that affect their activities. For example, Schiff bases, which are common ligands for early transition metal ions (Erxleben, 2018; Tadele and Tsega, 2019), can hydrolyze under biologically relevant conditions with the formation of aldehyde and amine components (Cordes and Jencks, 1962; Pessoa and Correia, 2019), the former being re-aminated with the amine groups of compounds contained in CCM (Levina et al., 2024). The extent of such reactions and their roles in biological activities of organic molecules in cell-based assays are often ignored.

Catechol (1,2-dihydroxybenzene) moieties are commonly found in natural bioactive compounds, including catecholamines (such as dopamine, a ubiquitous mammalian neurotransmitter) (van Bergeijk et al., 2022), plant metabolites (phenolic acids, such as caffeic acid, and flavonoids, such as quercetin or luteolin) (Pavlíková, 2022; Walencik et al., 2024) and siderophores that are used to harvest essential metal ions from the environment (such as enterobactin) (Liu et al., 2023). Some of these compounds, particularly flavonoids, are widely studied for their diverse medicinal properties, predominantly antioxidant and cancer-preventing activities (Hasnat et al., 2024). Deprotonated catechol moieties can efficiently bind to essential and biologically active transition metal ions, such as Cu(II), Fe(III) or V(V/IV) (Pierpont, 2001; Kundu et al., 2013; Walencik et al., 2024), which can lead to a reverse in biological activity mode, such as antioxidant catechols and flavonoids that become pro-oxidant in the presence of Cu(II) or Fe(III) ions (Hepel et al., 2012; Jomová et al., 2019; Rajashekar, 2023). Common biological thiols, such as glutathione (GSH), (Forman et al., 2009; Kennedy et al., 2020), play a major role in the biological activity of catechols (Gao et al., 2018), including the formation of catechol-thiol adducts (Li et al., 2016).

Complexes of V(V/IV) with catechol and flavonoid ligands are studied as models of catechol oxidase enzymes (Yin and Finke, 2005a; Yin and Finke, 2005b) and potential antidiabetic, antimicrobial and anticancer drugs (Shukla et al., 2006; Etcheverry et al., 2008; Pessoa et al., 2015; León et al., 2016a; Crans et al., 2018; Selvaraj and Krishnan, 2021; Ścibior, 2022; Naso et al., 2023). Our groups have explored the use of these complexes, including mixed-ligand $[V^{V}OL(cat)]$ and non-oxido $[V^{V}(cat)_3]^-$ complexes (where L is a Schiff base and cat is a doubly-deprotonated catechol), as anticancer drugs (Crans et al., 2019; Griffin et al., 2019; Levina et al., 2020; Murakami et al., 2022; Kostenkova et al., 2023; Levina et al., 2023; Haase et al., 2024; Bates et al., 2025). The mode of action of these complexes can involve the decomposition in cell culture medium on seconds to hours timescale, dependent on the nature of the catechol ligand (Murakami et al., 2022; Kostenkova et al., 2023; Haase et al., 2024), and secondary reactions of the released catechols with the released V(V) species (Levina et al., 2023). For more stable complexes that have substantial cellular uptake before decomposition, subsequent reactions of this type can occur intracellularly (Levina et al., 2023). Some such complexes showed high promise for the use in novel cancer treatments, such as intratumoral injections with or without oncolytic viruses (Selman et al., 2018; Bergeron et al., 2019; McAusland et al., 2021; Levina et al., 2022; Xu et al., 2024). To fine-tune the structures of these complexes and to propose optimal treatment conditions, a better understanding of the *in vitro* anticancer activities of free catechol ligands is desired. This work presents a detailed study of the speciation in cell culture medium and the anti-proliferative activity in cancer cell lines of a simple model substituted catechol, 3,5-di-*tert*-butylcatechol ($dtbH_2$), and its oxidized analogue, 3,5-di-*tert*-butyl-*o*-quinone (dtbQ), in the presence or absence of GSH as one of the most abundant biological reductants (Forman et al., 2009; Kennedy et al., 2020). This ligand was chosen as its complexes showed optimal anti-proliferative activities of all of the catecholato complexes studied (Crans et al., 2019; Levina et al., 2020; Murakami et al., 2022; Kostenkova et al., 2023; Levina et al., 2023; Haase et al., 2024).

2 Materials and methods

2.1 Compounds and analytical techniques

The following compounds from Merck were used as received: 3,5-di-*tert*-butylcatecol ($dtbH_2$, >98%, D45800), 3,5-di-*tert*-butyl-o-benzoquinone (dtbQ, >98%, 157457), L-glutathione reduced form (GSH, >98%, G6013), and L-histidine monochloride monohydrate (His, >99%, H5659). Other chemicals of analytical or higher purity grade were purchased from Merck, and water was purified by the MilliQ technique.

Reactions of $dtbH_2$ and dtbQ (0.10 mM) in neutral aqueous media under ambient atmosphere at 310 K were studied by

electronic absorption (UV-vis) spectroscopy in either phosphate buffered saline (PBS, containing 150 mM NaCl and 20 mM phosphate buffer, pH 7.4), or in cell culture medium without phenol red (Thermo Fisher Scientific, Cat. No. 31053–028) that was fully supplemented according to the conditions of cell assays (see below), and additionally supplemented with 2-[4-(2-hydroxyethyl)piperazin-1-yl]ethanesulfonic acid (HEPES, 10 mM) to maintain pH 7.4 outside of a high-CO_2 incubator (Levina et al., 2017). The pH values of PBS and media were checked immediately before use with an Activon 210 ionometer that was equipped with AEP 321 glass/Ag/AgCl electrode and calibrated daily using standard pH solutions (Aldrich). Stock solutions of $dtbH_2$ or dtbQ [10 mM in dimethyl sulfoxide (DMSO)], GSH (0.50 M in H_2O, containing 0.50 M NaOH to neutralize the free COOH group of GSH) or His (0.50 M in H_2O) were prepared on the day of experiments and diluted 100-fold with the medium or PBS immediately before the measurements. The UV-vis spectra were acquired in the 250–550 nm range (resolution, 0.5 nm) on a Specord S600 diode-array spectrometer (Analytic Jena, Germany) that was equipped with a HP89090A Peltier temperature controller. Background spectra were collected for solutions that contained all the components except for $dtbH_2$ or dtbQ. Global kinetic analysis of time-dependent spectra (Lay and Levina, 1996; Levina et al., 2023) was performed by ProKineticist software (version 1.06, Applied Photophysics, Leatherhead, UK, 2001).

Typical reaction mixtures for low-resolution electrospray ionization mass spectrometry (ESI-MS) were prepared by mixing 20 μL of 10 mM solutions of $dtbH_2$ or dtbQ in dimethylformamide (DMF) with 2.0 μL of 0.10 M aqueous solutions of GSH and/or His. The reaction mixtures were kept for 1 h at 295 K, then diluted 100-fold with HLPC-grade MeOH, and ESI-MS or UV-vis (see above) data were immediately collected. The use of DMF in these experiments was required because of the incompatibility of DMSO with ESI-MS conditions. The ESI-MS data were collected on a Bruker amaZon SL spectrometer, using the following parameters: nebulizer pressure, 27.3 psi; spray voltage, 4.5 kV; capillary temperature, 453 K; N_2 flow rate, 4 L min^{-1}; *m/z* range, 100–1,000 (alternating positive- and negative-ion modes). Analyzed solutions (5.0 μL) were injected into a flow of MeOH (flow rate, 0.30 mL min^{-1}). Acquired spectra were the averages of 100–200 scans (scan time, 10 ms). Simulations of the mass spectra were performed using IsoPro software (version 3.0, M. Senko, Sunnyvale, CA, United States, 1998).

2.2 Cell culture and proliferation assays

Pre-sterilized media and sterile plasticware used in cell culture were purchased from Thermo Fisher Scientific Australia. The well-established human cancer cell lines: T98G (glioblastoma multiforme, CRL-1690) and A549 (human lung carcinoma, CCL-185) were purchased from the American Type Culture Collection (ATCC) and used at passages six to ten. The cells were cultured using standard techniques (Freshney, 2016) in Advanced DMEM (Cat. No. 12491–015), supplemented with L-glutamine (2.0 mM), antibiotic-antimycotic mixture (100 U mL^{-1} penicillin, 100 mg mL^{-1} streptomycin and 0.25 mg mL^{-1} amphotericin B) and fetal calf serum (FCS; heat-inactivated; 2% vol). For proliferation experiments, cells were seeded in 96-well plates at an initial density of 1.0×10^3 viable cells per well in 100 μL medium and left to attach overnight.

Cell proliferation was measured in 72 h assays using either fully supplemented growth medium or the medium additionally supplemented with a physiological intracellular concentration (5.0 mM) (Forman et al., 2009) of GSH. The GSH-supplemented media were prepared immediately before use by dissolving solid GSH in fully supplemented medium, neutralizing the resultant solution to pH 7.4 with 5.0 M NaOH (controlled by the color of the phenol red indicator) and filtering through a sterile 0.22 μm pore membrane (Merck SLGP044RS). Stock solutions of $dtbH_2$ or dtbQ (10 mM in DMSO) were serially diluted two-fold with DMSO and then added to cell culture media so that all the treatments, including controls, contained 1.0% (vol.) DMSO, which was well tolerated by the cells (Ilieva et al., 2021). The treatment compounds were applied in a series of nine two-fold dilutions, starting from 100 μM, plus the vehicle control. Cell culture media containing the treatment compounds at the required final concentrations were either added to the cells within 1 min (fresh solutions) or left in cell culture incubator (310 K, 5% CO_2) for 24 h prior to the cell treatments (aged solutions) (Griffin et al., 2019; Levina et al., 2020; Murakami et al., 2022; Kostenkova et al., 2023; Levina et al., 2023). Each treatment included six replicate wells and two background wells that contained the same components except the cells. After 72 h incubation with the treatment compound, the treatment medium was removed and the medium containing MTT reagent (1-(4,5-dimethylthiazol-2-yl)-3,5-diphenylformazan, Sigma M5655; 1.0 mg mL^{-1}; prepared immediately before use) (Sylvester, 2011) was added. After 4–6 h incubation with MTT reagent, the medium was removed, the blue formazan crystals were dissolved in 0.10 mL per well of DMSO, and the absorbance at 600 nm was measured using a Clariostar plate reader. The IC_{50} values were calculated using Origin Pro software (2022 version, OriginLab, Northampton, MA, United States). Consistent results were obtained in at least two independent experiments, using different batches of cells and different stock solutions.

3 Results

3.1 Reactions of $dtbH_2$ and dtbQ in cell culture medium and in model solutions

Changes in UV-vis spectra of $dtbH_2$ or dtbQ (0.10 mM) after the reactions with phosphate buffered saline (PBS) or cell culture medium (CCM) at pH 7.4 and ambient atmosphere at 310 K are shown in Figures 1A–C. At the beginning of the reaction in PBS, $dtbH_2$ and dtbQ showed distinct spectra with absorbance maxima at 280 nm and 415 nm, respectively (black and red lines in Figure 1A). After 24 h, both solutions showed the 415 nm peak at ~30–40% of maximal intensity (blue and green lines in Figure 1A. These data indicate that $dtbH_2$ is slowly oxidized to dtbQ by ambient oxygen at pH 7.4, while a general decrease in absorbance intensities in the spectrum of dtbQ is most likely due to its slow precipitation.

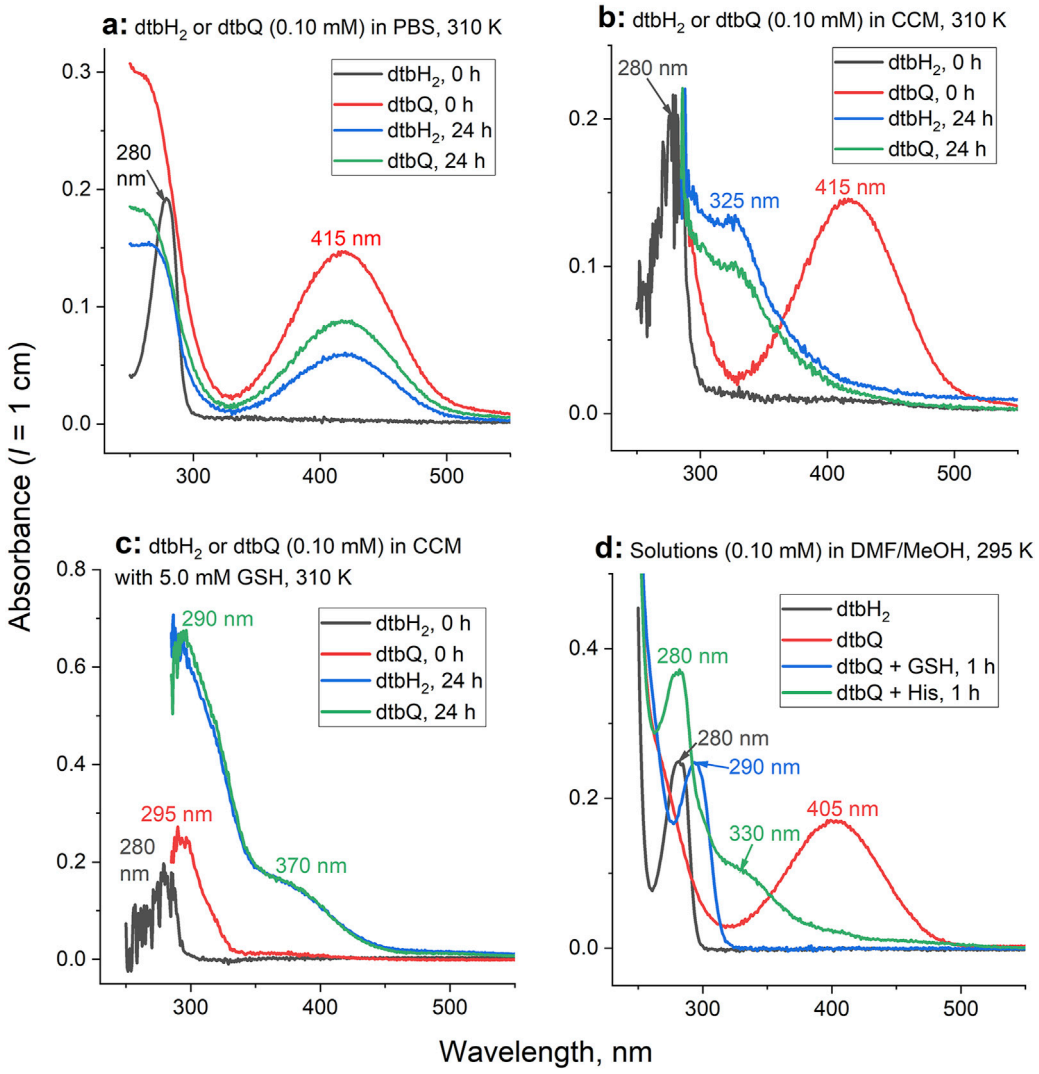

FIGURE 1
Typical time changes of UV-vis spectra for the reactions of $dtbH_2$ or dtbQ (0.10 mM) with or without biological nucleophiles in aqueous or organic solvents. **(A)** Reactions in PBS at 310 K (additional data are shown in Supplementary Figure S1). **(B)** Reactions in cell culture medium (CCM) at 310 K. **(C)** Reactions in CCM in the presence of 5.0 mM GSH at 310 K. **(D)** Reactions of 10 mM $dtbH_2$ or dtbQ in DMF in the presence or absence of 10 mM GSH or His at 295 K, followed by 100-fold dilution with MeOH (matching the conditions of ESI-MS, Figure 2).

The initial spectra of $dtbH_2$ and dtbQ in CCM were similar to those in PBS (black and red lines in Figure 1B). Unlike for the reactions in PBS, the characteristic absorbance peak of dtbQ disappeared completely after the reaction with cell culture medium for 24 h, and the distinct spectra of $dtbH_2$ and dtbQ converged into similar spectra featuring a shoulder at 325 nm (blue and green lines in Figure 1B). Reaction of dtbQ with CCM that contained 5.0 mM GSH led to immediate disappearance of the original absorbance at 415 nm and formation of a new absorbance maximum at 295 nm (red line in Figure 1C). After 24 h reaction with GSH-containing CCM both $dtbH_2$ and dtbQ converged into the same product (blue and green lines in Figure 1C) that was distinct from the product formed in the absence of GSH by higher absorbance intensity and shoulders at 290 nm and 370 nm. Similar, but not identical, spectra were observed after the reactions of $dtbH_2$ or dtbQ with PBS that contained 5.0 mM GSH and/or 5.0 mM His (as a model of amino acids contained in CCM) (Levina et al., 2017) for 24 h at 310 K, as shown in Supplementary Figure S1. Notably, when both GSH and His were added to PBS, the spectra of the reaction products were identical to those with GSH alone.

Spectral changes similar to those observed for the reactions of $dtbH_2$ or dtbQ with 50-fold molar excess of GSH or His in PBS (Supplementary Figure S1) were also observed for the reactions of equimolar quantities of dtbQ with GSH or His (10 mM each) in DMF solutions for 1 h at 295 K, followed by 100-fold dilution with MeOH immediately before recording the spectra (Figure 1D). The spectra of $dtbH_2$ and dtbQ alone resembled those in aqueous media (black and red lines in Figure 1D). Reaction of dtbQ with GSH led to formation of a new absorbance maximum at 290 nm, while the reaction of dtbQ with His led to a maximum at 280 nm and a shoulder at 330 nm (blue and green lines in Figure 1D). No further spectral changes for the reaction

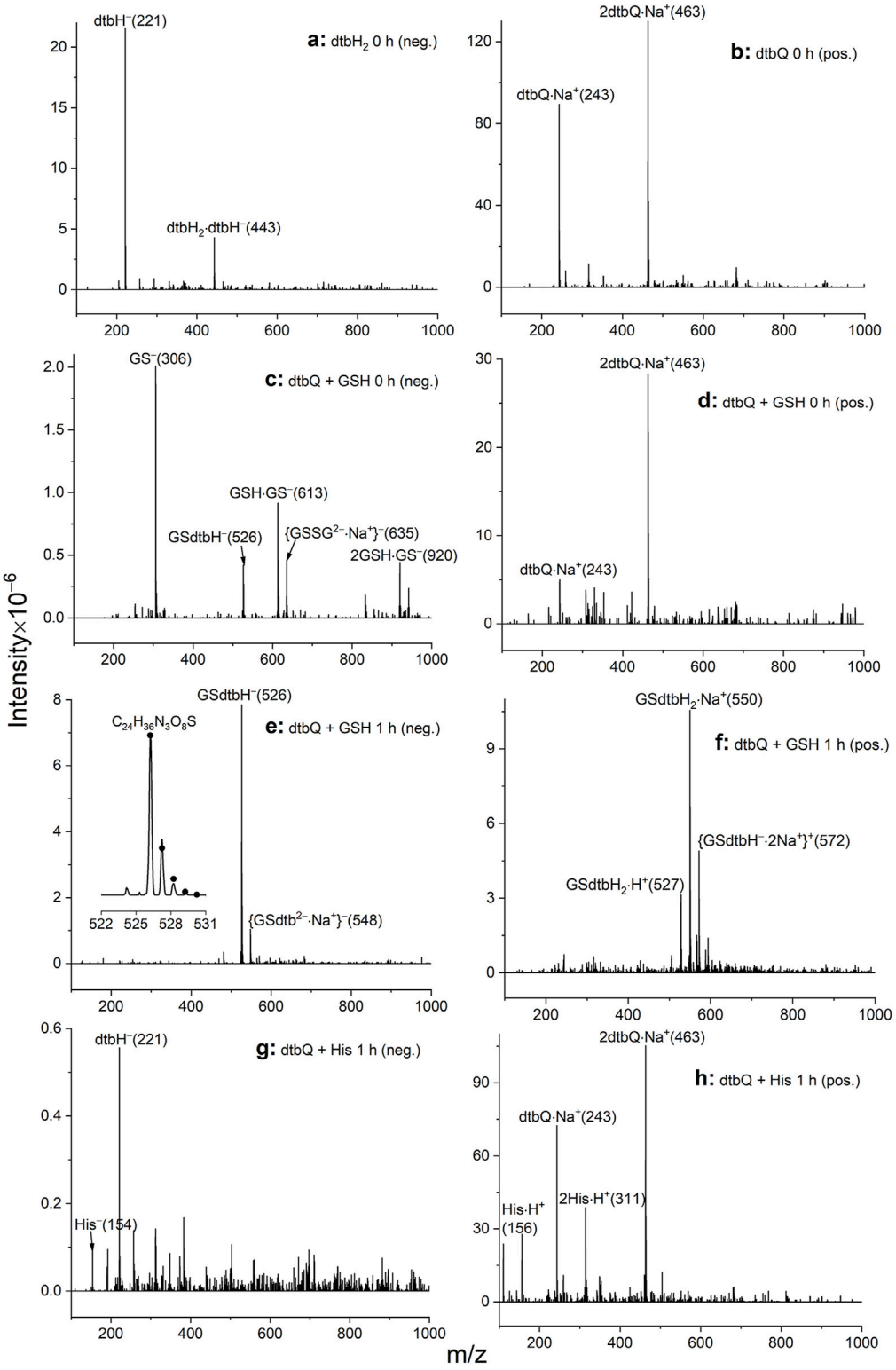

FIGURE 2
Typical ESI-MS data for the reactions of 10 mM $dtbH_2$ or dtbQ with or without 10 mM GSH or His in DMF solutions for 0–1 h at 295 K, followed by 100-fold dilution with MeOH. Assignments of the main peaks are shown together with the *m/z* values of the main peaks in the isotopic distribution (in parentheses). **(A)** Negative-ion mode for $dtbH_2$ alone (no significant signals in the positive-ion mode). **(B)** Positive-ion mode for dtbQ alone (no significant signals in the negative-ion mode). **(C)** Negative-ion mode for dtbQ + GSH immediately after mixing. **(D)** Positive-ion mode for dtbQ + GSH immediately after mixing. **(E)** Negative-ion mode for dtbQ + GSH after 1 h of reaction; experimental (line) and simulated (dots) isotopic distribution of the main signal is shown in the inset. **(F)** Positive-ion mode for dtbQ + GSH after 1 h of reaction. **(G)** Negative-ion mode for dtbQ + His after 1 h of reaction. **(H)** Positive-ion mode for dtbQ + His after 1 h of reaction.

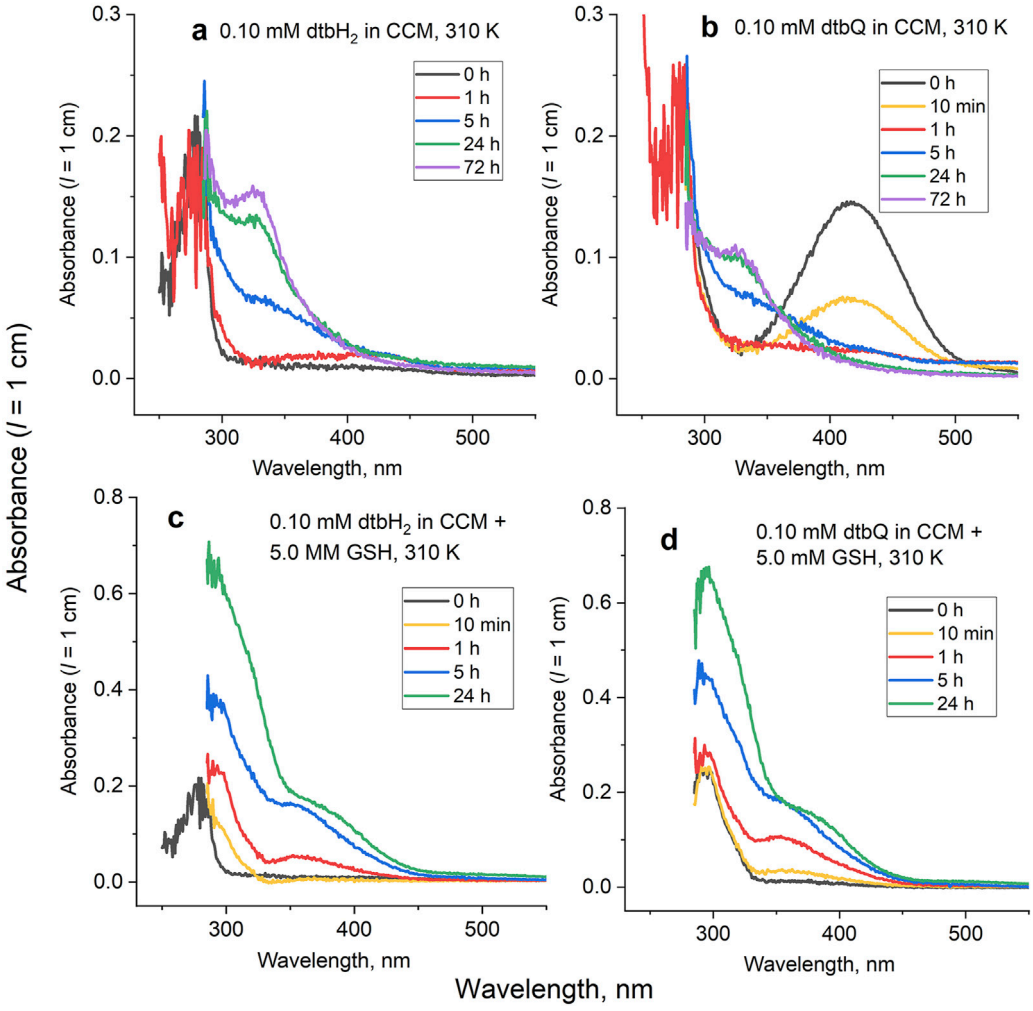

FIGURE 3
Typical time-dependent UV-vis spectra for the reactions of $dtbH_2$ or dtbQ (0.10 mM) in cell culture medium (CCM) in the presence or absence of 5.0 mM GSH for 0–72 h at 310 K. Data of global kinetic analyses are shown in Supplementary Figures S2, S3. Reactions of **(A)** $dtbH_2$ in the absence of GSH; **(B)** dtbQ in the absence of GSH; **(C)** $dtbH_2$ in the presence of GSH; **(D)** dtbQ in the presence of GSH.

products of dtbQ with GSH or His in DMF were observed after 24 h reaction at 295 K, and no significant changes in the spectra of $dtbH_2$ were observed in the presence of either GSH or His (all at 10 mM in DMF) for up to 24 h. Neither GSH nor His showed a significant absorbance in the wavelength range used (250–550 nm). Similarly to the reactions in PBS, the spectra of the reaction products of dtbQ with both GSH and His (all 10 mM in DMF) were not significantly different from those for the reaction with GSH only.

Reaction conditions used to collect the UV-Vis spectra in Figure 1D (reactions of 10 mM compounds in DMF, followed by 100-fold dilution with MeOH) were used for the analysis of reaction products by ESI-MS (Figure 2). In the absence of GSH or His, signals of deprotonated $dtbH_2$ could only be observed in the negative-ion mode (Figure 2A), while the signals of dtbQ were only observed in the positive-ion mode as Na^+ adducts (Figure 2B). Reaction products of dtbQ and GSH immediately after mixing (Figures 2C, D) showed the signals of dtbQ in the positive-ion mode and deprotonated GSH in the negative-ion mode, as well as a new signal at m/z = 526 (negative-ion mode), which corresponded to the oxidative coupling product of GSH and dtbQ (Li et al., 2016; Lyu et al., 2019; Alfieri et al., 2022). This product became dominant in both positive- and negative-ion modes after 1 h of reaction (Figures 2E, F). By contrast, no new signals of reaction products were observed for the reaction of dtbQ and His for up to 24 h (illustrated in Figures 2G, H), despite the observed changes in UV-vis spectra under these conditions (red and green lines in Figure 1D).

Typical time-dependent UV-vis spectra for the reactions of $dtbH_2$ or dtbQ (0.10 mM) with CCM in the presence or absence of 5.0 mM GSH at 310 K are shown in Figure 3, and full kinetic analysis is presented in Extended Data Supplementary Figures S2, S3. For the reaction of $dtbH_2$ in the medium without added GSH (Figure 3A), the initial spectrum (black line) was similar to that of $dtbH_2$ in PBS (Figure 1A), except for the high noise level due to strong absorbance of CCM below 300 nm. Within the first 1 h of reaction, partial oxidation of dbH_2 to dtbQ (up to 10% mol.) was evident from increased absorbance around 400 nm (red line in Figure 3A). For the next 5–10 h, a shoulder at ~350 nm was formed (blue line in Figure 3A), which resembled that observed

TABLE 1 Anti-proliferative activities in T98G (human glioblastoma) and A549 (human lung carcinoma) cell lines at 72 h assays.

Compound and medium [a]	IC_{50}, μM (T98G)[b]	IC_{50}, μM (A549)[b]
$dtbH_2$, no GSH, fresh	6.3 ± 0.3	7.7 ± 0.6
$dtbH_2$, no GSH, aged	31 ± 2	45 ± 3
dtbQ, no GSH, fresh	4.0 ± 0.5	5.7 ± 0.5
dtbQ, no GSH, aged	39 ± 1	57 ± 4
$dtbH_2$, GSH, fresh	7.9 ± 0.5	4.8 ± 0.8
$dtbH_2$, GSH, aged	12.1 ± 0.7	8.9 ± 1.2
dtbQ, GSH, fresh	8.5 ± 0.9	4.3 ± 0.7
dtbQ, GSH, aged	10.2 ± 0.9	6.9 ± 1.3
cisplatin, no GSH, fresh	39 ± 1 [c]	5.7 ± 0.5 [c]
cisplatin, no GSH, aged	>50 [c]	25 ± 1 [c]
[$V^{V}O$(HSHED) (dtb)],[d] no GSH, fresh	2.5 ± 0.1 [c]	3.9 ± 0.2 [c]
[$V^{V}O$(HSHED) (dtb)],[d] no GSH, aged	20 ± 1.5 [c]	17.6 ± 0.7 [c]

[a]Cell treatments were performed for 72 h in Advanced DMEM, containing 2% FCS, in the presence or absence of added GSH (5.0 mM). For fresh treatments, dilutions of the compounds (0–100 μM) in cell culture medium were added to the cells within 1 min after the preparation. For aged treatments, dilutions of the compounds (0–100 μM) in cell culture medium were pre-incubated at 310 K and 5% CO_2 for 24 h, then added to the cells for further 72 h.

[b]Concentrations of the compounds that caused 50% decrease in cell viability in 72 h assays. Values are the means and standard deviations of six replicate wells. Typical concentration-viability curves are shown in Figure 4.

[c]Data from (Levina et al., 2020).

[d]A mixed-ligand V(V) complex with a Schiff base (HSHED = *N*-(salycylideneaminato)-*N'*-(2-hydroxyethyl)ethane-1, 2-diamine(1−)) and doubly-deprotonated $dtbH_2$ ligands (Levina et al., 2020).

for the reaction of $dtbH_2$ with 5.0 mM His in PBS solution (Supplementary Figure S1A). A final spectrum, featuring a shoulder at 325 nm, was formed by 24 h and did not change significantly for up to 72 h of reaction (green and purple lines in Figure 3A). For the reaction of dtbQ under the same conditions, the characteristic absorbance of dtbQ at 415 nm nearly disappeared within the first hour of reaction (black, yellow and red lines in Figure 3B), and further spectral changes closely resembled those for $dtbH_2$ (blue, green and purple lines in Figure 3B). These results indicate that dtbQ is efficiently reduced to $dtbH_2$ in air-saturated CCM in the absence of added reductants, which is in stark contrast with the data for PBS solutions, where $dtbH_2$ is oxidized to dtbQ under the same conditions (Figure 1A). The redox equilibrium established in CCM includes oxidation of $dtbH_2$ to dtbQ by aerial oxygen and reduction of dtbQ to $dtbH_2$ by medium components, which results in the formation of ~90% $dtbH_2$ and ~10% dtbQ within ~1 h at 310 K starting from either compound (Supplementary Figure S2).

Time courses of the reactions of $dtbH_2$ or dtbQ with CCM containing 5.0 mM GSH (Figures 3C, D) closely followed each other, except that a new spectrum with absorbance maximum at 290 nm was formed immediately after the addition of dtbQ to the medium or within 10 min in the case of $dtbH_2$ (yellow lines in Figures 3C, D). Further changes for the both compounds involved an increase in absorbance intensity at 290 nm and formation of shoulders at 350–370 nm (red, blue and green lines in Figures 3C, D). These data indicate that both $dtbH_2$ and dtbQ convert to GSH-$dtbH_2$ adducts (see the ESMS data in Figure 2E) under these conditions.

3.2 Anti-proliferative activities in human cancer cells of $dtbH_2$, dtbQ and their reaction products in cell culture media

The anti-proliferative activities of $dtbH_2$ or dtbQ (0.4–100 μM) or their decomposition products in the presence or absence of added GSH (5.0 mM) in 72 h assays were compared in two well-established human cancer cell lines, T98G (glioblastoma) and A549 (lung cancer). Both cell lines were used previously to test the anti-proliferative activities of V(V) complexes with catecholato ligands (Levina et al., 2020; Murakami et al., 2022; Kostenkova et al., 2023; Haase et al., 2024). As in the previous studies of V(V) catecholato complexes (Griffin et al., 2019; Levina et al., 2020; Murakami et al., 2022; Kostenkova et al., 2023; Levina et al., 2023), the compounds were either mixed with CCM within 1 min of cell treatment (fresh solutions) or reacted with CCM at final dilution concentrations for 24 h at 310 K before the treatment (aged solutions). A summary of IC_{50} values under different conditions is given in Table 1, and typical concentration-viability curves are shown in Figure 4.

Fresh solutions of either $dtbH_2$ or dtbQ in the presence or absence of GSH showed high activity (IC_{50} ~ 5–10 μM, Table 1) that was comparable (for A549 cells) or higher (for T98G cells) than that of a standard anti-cancer drug, cisplatin, under the same conditions (Table 1) (Levina et al., 2020). Aging of $dtbH_2$ or dtbQ in CCM without GSH led to 5-10-fold decrease in activity in both cell lines (Table 1; Figures 4A–D). By contrast, in the presence of GSH, aging of the compounds only led to a minor decrease in activity (Table 1; Figures 4E–H). Notably, the activity of cisplatin also reduced on aging in cell culture medium (Table 1) (Levina et al., 2020), likely due to the covalent Pt(II) binding to albumin (Gibson, 2009).

10.3389/fchbi.2025.1547323

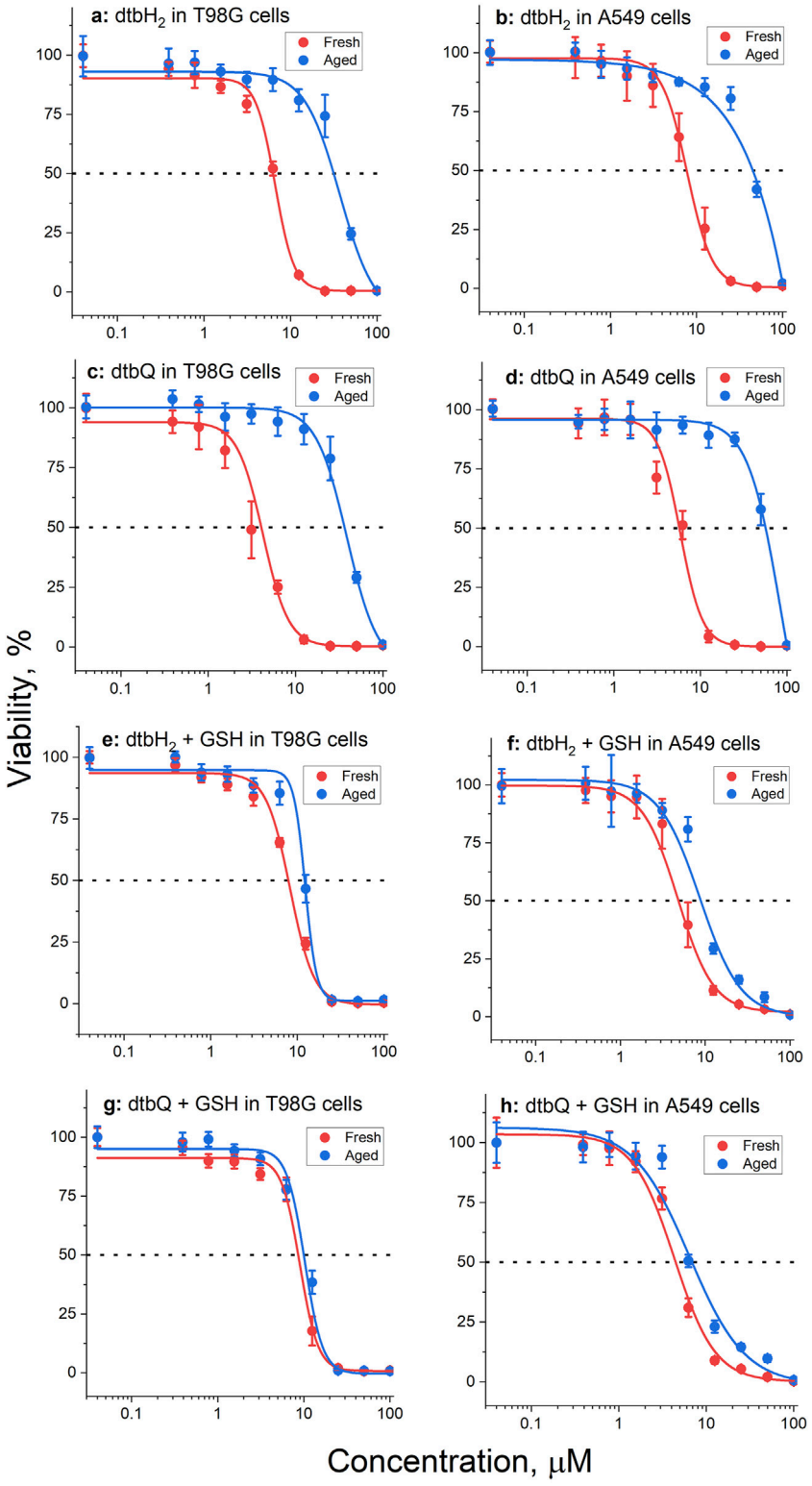

FIGURE 4
Typical concentration-viability curves (72 h treatments, MTT assays) of T98G or A549 cells with fresh (red lines) or aged (pre-incubated with medium for 24 h before the cell treatment, blue lines) solutions of $dtbH_2$ or dtbQ (0–100 μM) in the presence or absence of 5.0 mM GSH. The dots and error bars represent the means and standard deviations of six replicate wells. The corresponding IC_{50} values are listed in Table 1. Conditions: **(A)** $dtbH_2$ in T98G cells, no GSH; **(B)** $dtbH_2$ in A549 cells, no GSH; **(C)** dtbQ in T98G cells, no GSH; **(D)** dtbQ in A549 cells, no GSH; **(E)** $dtbH_2$ in T98G cells, with GSH; **(F)** $dtbH_2$ in A549 cells, with GSH; **(G)** dtbQ in T98G cells, with GSH; **(H)** dtbQ in A549 cells, with GSH.

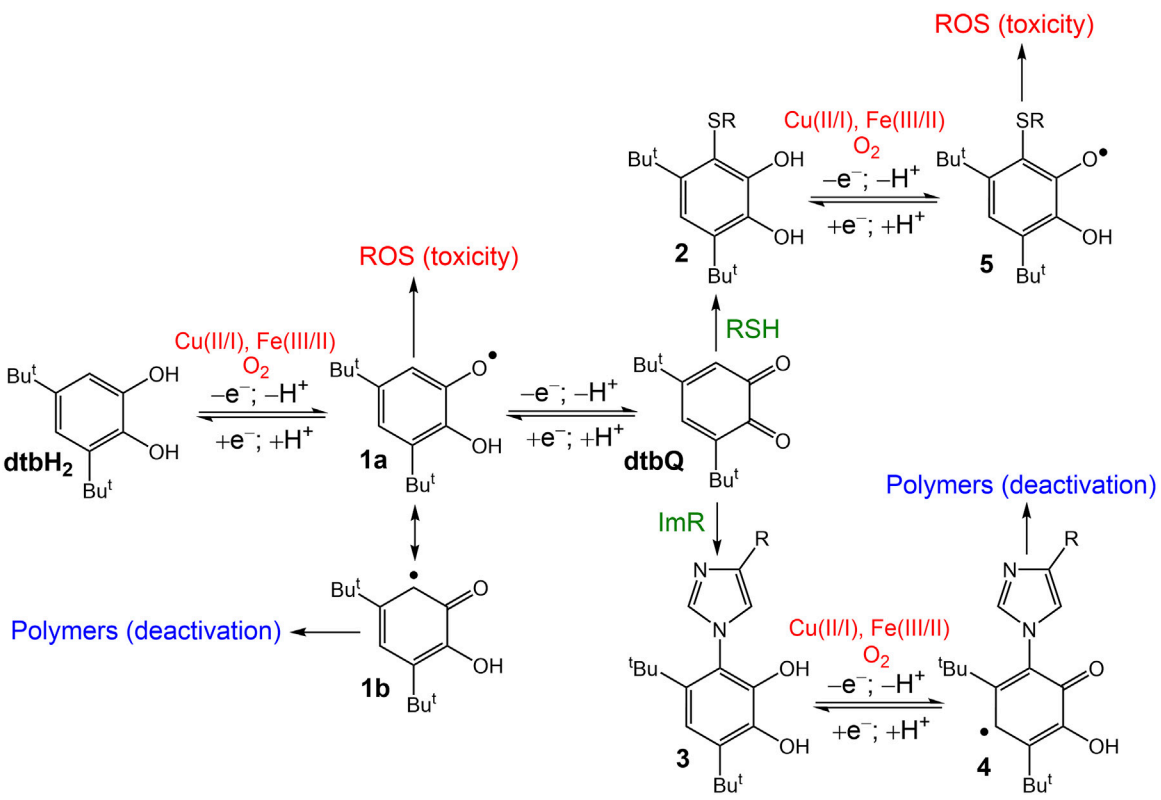

SCHEME 1
Proposed reaction mechanism of $dtbH_2$ or dtbQ in biological media under normoxic conditions. ROS are reactive oxygen species; RSH are biological thiols, such as GSH; and ImR are imidazole-containing compounds, such as free His or His residues of proteins.

4 Discussion

4.1 Reactivities and anti-proliferative activities of $dtbH_2$ and dtbQ in cell assays

To our knowledge, this is the first report of high anti-proliferative activity of $dtbH_2$ and its close analogue, dtbQ, in human cancer cell lines, although the activity of unsubstituted catechol has been reported (Pereira et al., 2004). The absence of previous data on the activity of $dtbH_2$ in cell culture studies can be due to its rapid deactivation in CCM (Table 1). To observe the activity, it was essential that the dilutions of $dtbH_2$ in CCM were prepared within ~1 min before the addition to cells. Furthermore, the rapid decomposition in biological media can possibly explain that no evidence of toxicity was observed in mice of both $dtbH_2$ and its V(V) complex when acutely exposed to a single dose of 300 mg kg^{-1} for 14 d (Lima et al., 2021). The toxicological results obtained with biochemical and hematological analyses did not show significant changes in kidney and liver parameters when compared with reference values (Lima et al., 2021). High reactivity in CCM is also likely to contribute to the conflicting literature data on the biological activities of natural catechol-containing molecules, such as quercetin (Xu et al., 2019; Someya et al., 2024).

A proposed reaction mechanism of $dtbH_2$ and dtbQ in CCM with or without added GSH that can explain the observed spectral and biological activity changes is outlined in Scheme 1.

The redox equilibrium between the catechol ($dtbH_2$), semiquinone (**1a**) and quinone (dtbQ) was shifted towards $dtbH_2$ under normal cell culture conditions, but up to 10% mol. dtbQ was present in the mixture of the oxidized and reduced forms (Figure 3A). The redox reactions are likely to be catalyzed by trace metal ions present in the medium, such as Fe(III/II) and Cu(II/I) (Scheme 1) (Hepel et al., 2012; Jomová et al., 2019; Rajashekar, 2023). Formation of semiquinone radicals can trigger metal-catalyzed radical chain reactions and the formation of reactive oxygen species (ROS) (Lyu et al., 2019), which is a likely main reason for the anti-proliferative activity of $dtbH_2$ (marked with red color in Scheme 1) and of biological catechols, such as quercetin (Someya et al., 2024). Formation of a tautomeric semiquinone radical, **1b**, can lead to polymerization products (Lyu et al., 2019), which is one of the likely reasons for deactivation of $dtbH_2$ and dtbQ after aging in cell culture medium with no added GSH (Table 1; marked with blue color in Scheme 1). Unlike for the redox reactions of $dtbH_2$ and dtbQ in CCM, the equilibrium is shifted towards dtbQ in PBS solutions under the same conditions (Figure 1A). This difference emphasizes the need to perform reactivity and speciation studies in cell culture medium, rather than in simple aqueous buffers, to explain the results of cell-based assays (Levina et al., 2017).

Reactions of dtbQ with nucleophiles (Li et al., 2016; Lyu et al., 2019; Alfieri et al., 2022) in cell culture medium, including biological thiols and imidazole groups (designated as RSH and ImR, respectively, in Scheme 1), can lead to oxidative coupling products (**2** and **3** in Scheme 1). In the presence of comparable

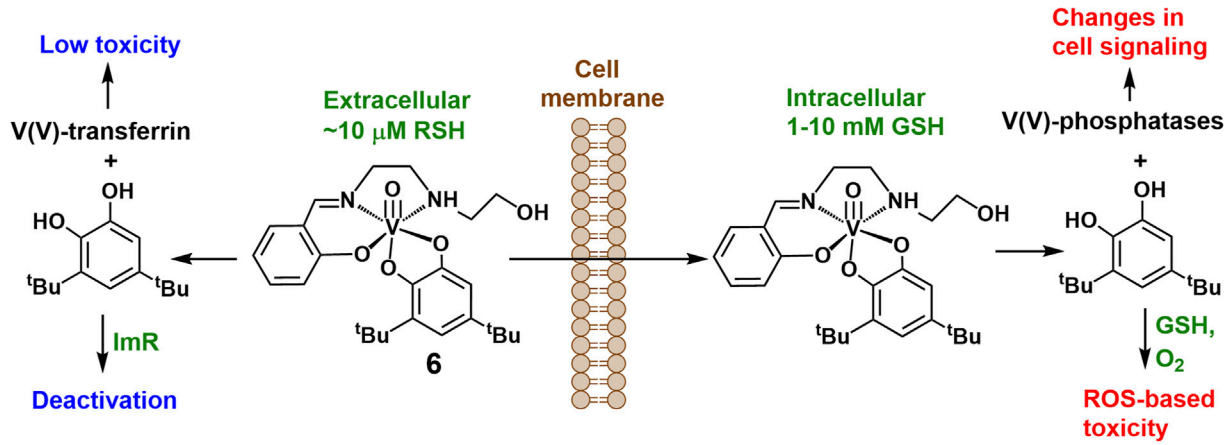

SCHEME 2
Proposed roles of V(V) species and the free $dtbH_2$ ligand following the extra- and intracellular decomposition of an unstable but highly cytotoxic [$V^{V}O$(HSHED) (dtb)] complex (Levina et al., 2020).

concentrations of thiols and imidazole groups, the reaction of dtbQ with the former is favored, as shown by UV-vis spectroscopy of reaction products with both GSH and His (5.0 mM each) in PBS solutions (Supplementary Figure S1). Also, the reaction product of dtbQ and GSH was easily detected by ESI-MS (Figures 2C, D), unlike for those of the reaction with His (Figures 2G, H). This can be due to the formation of semiquinone radicals of $dtbH_2$-His adducts (**4** in Scheme 1), followed by polymerization. Ready polymerization of these adducts can also explain the absence of their signals in ESI-MS data (Figures 2G, H). By contrast, the thiol addition product, **2**, is more likely to undergo further redox reactions with the formation of semiquinone radicals (**5** in Scheme 1) and ROS, leading to anti-proliferative activity. This is consistent with the absence of significant decrease in anti-proliferative activity of $dtbH_2$ and dtbQ after aging in CCM in the presence of 5.0 mM GSH (Table 1). The ability of a potent antioxidant, GSH, to enhance the ROS-related activity of $dtbH_2$ and dtbQ is counterintuitive, but it can be important for the medicinal use of these compounds in the reducing environment of solid tumors (Chen et al., 2023).

4.2 Implications for biological activities of metal-catecholato complexes

It is important to establish a relationship between the anti-proliferative activities of free $dtbH_2$ and metal complexes that contain $dtbH_2$ as a ligand and can release it under biological conditions, such as a V(V)-Schiff base-catecholato complex, [$V^{V}O$(HSHED) (dtb)] (**6** in Scheme 2), where HSHED is *N*-(salycylideneaminato)-*N′*-(2-hydroxyethyl)ethane-1,2-diamine(1−)) and dtb is doubly-deprotonated $dtbH_2$ (Levina et al., 2020; Levina et al., 2023). The complex decomposed within minutes in neutral aqueous media with the release of free $dtbH_2$ (Levina et al., 2023). Like $dtbH_2$, the complex was 5-10-fold more active in the fresh state than after 24 h aging in cell culture medium at 310 K (two bottom rows in Table 1) (Levina et al., 2020). However, the activities of the fresh complex in both T98G and A549 cells were 2-3-fold higher than that of fresh $dtbH_2$ (Levina et al., 2020). Cell treatments with fresh **6** led to cellular V content that was at least 100-fold higher than the background values, which is consistent with the activity being due to rapid cellular uptake of the intact V(V) complex (Levina et al., 2020; Levina et al., 2023). Based on the kinetic studies in CCM in the absence of added GSH (Figure 3A and Supplementary Figure S2), the released $dtbH_2$ is expected to bind rapidly to nucleophiles in cell culture medium, leading to its deactivation (Schemes 1, 2). Therefore, the release of $dtbH_2$ outside of the cells is unlikely to play a major role in the activity of lipophilic V(V) complexes, such as **6**, that act by rapid cellular uptake of the intact complex (Levina et al., 2020; Murakami et al., 2022; Kostenkova et al., 2023; Levina et al., 2023).

The observed effect of high thiol concentration (5.0 mM GSH) on the activity of $dtbH_2$ in cell assays (Table 1; Figure 4) brings the question about the role of GSH in the intracellular reactions of **6** and other metal-catecholato complexes (Crans et al., 2010). Under normal physiological conditions, concentrations of reduced thiols in the blood plasma are low (~10 μM), because the cysteine residues of albumin and other plasma proteins predominantly occur in the oxidized state (Turell et al., 2013). By contrast, typical concentrations of reduced GSH in cancer cells are 1–10 mM and are up to 100-fold higher than those in normal cells (Forman et al., 2009; Kennedy et al., 2020). Therefore, $dtbH_2$ that is released from **6** extracellularly is likely to be deactivated though oxidation to dtbQ and subsequent binding to imidazole-based nucleophiles (Schemes 1, 2). The released V(V) species (up to ~50 μM, which is relevant to the conditions of cell assays, Table 1) are likely to bind to transferrin (the main Fe(III) transport protein) in the blood plasma, which is known to reduce their cellular uptake and toxicity (Scheme 2) (Levina and Lay, 2020). Inside the cancer cells, the presence of high GSH concentrations is likely to promote the dissociation of **6** with the formation of free $dtbH_2$ and binding of the released V(V) species to proteins, including the active sites of protein tyrosine phosphatases, leading to changes in cell signaling (Scheme 2) (McLauchlan et al., 2015; Levina et al., 2017; Feng et al., 2022), while the oxidation of $dtbH_2$ to dtbQ and subsequent reactions with GSH can lead to ROS-based toxicity (Schemes 1, 2).

It has been reported that speciation is linked to the activity of V(V/IV) complexes with a variety of ligands, including flavonoids (Aureliano et al., 2023; Naso et al., 2023). As shown in Scheme 2, the

biological effects of decomposition products of **6** within cancer cells are likely to be caused by a combination of ROS-dependent (e.g., reactions of $dtbH_2$ oxidation products) and ROS-independent (e.g., V(V) binding to phosphatases) processes. This is consistent with the observed ~50% decrease in the anti-proliferative activity of **6** in MDA-MB-231 triple-negative breast cancer cells at 5.0 μM (the approximate IC_{50} at 72 h) under hypoxic (1% O_2) versus normoxic (20% O_2) conditions at the same V(V) concentration. The IC_{50} value of 1.9 μM in MDA-MB-231 cells under normoxic conditions (Levina et al., 2023) is close to those in Table 1 for the T98G and A549 cells under the same conditions. Therefore, efficient cellular uptake of **6** results in at least two independent toxicity pathways that can operate under both hypoxic and normoxic conditions. In effect, V(V)-$dtbH_2$ binding facilitates the cellular uptake of both the metal ion and the ligand, while inside the cells, they are likely to dissociate and act via independent pathways, as was proposed for Cu(II) complexes with diimine ligands, such as 1,10-phenanthroline and its derivatives (Nunes et al., 2020). Higher GSH concentrations in cancer vs. non-cancer cells can contribute to selectivity of action of V(V)-$dtbH_2$ complexes (Kostenkova et al., 2023). Similar considerations also apply to V(V/IV) complexes with flavonoid (Shukla et al., 2006; Etcheverry et al., 2008; León et al., 2016a; León et al., 2016b; Selvaraj and Krishnan, 2021; Ścibior, 2022; Naso et al., 2023), diimine (Le et al., 2017; Nunes et al., 2021) or 8-hydroxyquinoline (Choroba et al., 2020; Levina et al., 2024) ligands. The proposed role of the difference in free thiol concentrations between extra- and intracellular environment in the activation V(V)-catecholato complexes within the cells (Scheme 2) is reminiscent of the role that the difference in extra- and intracellular Cl^- concentrations plays in the activation of classical metal-based anticancer drugs, such as cisplatin (Gibson, 2009).

Thus, the experiments conducted here indicate that both the mechanisms of V(V) phosphatase inhibition, as well as the dtb-GSH adduct ROS generation is likely to be operative *in vivo* for the anti-cancer efficacy against migrating cancer cells and those in the outer layers region of tumors that will both be under normoxic conditions. However, it is possible that in the hypoxic region of solid tumors the V(V) phosphatase inhibition is the main mechanism that operates.

5 Conclusion

High anti-proliferative activity of a representative model of biological catechols, 3,5-di-*tert*-butylcatechol ($dtbH_2$) and its oxidized analogue, 3,5-di-*tert*-butyl-*o*-quinone (dtbQ), in common human cancer cell lines, T98G (glioblastoma) and A549 (lung carcinoma) has been demonstrated. The activity of $dtbH_2$ and dtbQ was likely due to radical chain reactions catalyzed by trace essential metal ions, such as Fe(III/II) and Cu(II/I). A redox equilibrium was established in cell culture medium (CCM) under the assay conditions between $dtbH_2$ (a major component) and dtbQ. The latter reacted with nucleophiles contained in CCM, such as imidazole groups of amino acids and proteins, leading to partial loss of activity within hours at 310 K. Addition of biological thiols, such as glutathione (GSH), to CCM, led to immediate formation of GSH-$dtbH_2$ adducts, which retained the high anti-proliferative activity due to the ability to carry radical chain reactions. Similar mechanisms are likely to operate within cancer cells, which contain millimolar GSH concentrations, following the uptake of metal complexes with catechol-based ligands, and contribute into the selectivity of action of these complexes in cancer vs. non-cancer cells. These results emphasize the importance of consideration of speciation that impact the systems reactivity, which will involve all the species that form in the system including the catechol ligand that is released when the metal complexes hydrolyze in the cell-based assays.

Data availability statement

The raw data supporting the conclusions of this article will be made available by the authors, without undue reservation.

Ethics statement

Ethical approval was not required for the studies on humans in accordance with the local legislation and institutional requirements because only commercially available established cell lines were used.

Author contributions

AL: Conceptualization, Data curation, Formal Analysis, Funding acquisition, Investigation, Methodology, Visualization, Writing–original draft, Writing–review and editing. DC: Conceptualization, Funding acquisition, Methodology, Project administration, Resources, Supervision, Writing–review and editing. PL: Conceptualization, Funding acquisition, Methodology, Project administration, Resources, Supervision, Writing–review and editing.

Funding

The author(s) declare that financial support was received for the research, authorship, and/or publication of this article. This research was funded by the Australian Research Council (P.A.L.), Discovery grant number DP210101632 and the Tour de Cure (P.A.L., D.C.C. and A.L.) grant number RSP-317-202. D.C.C. thanks the Colorado State University and the Arthur Cope Foundation for partial support.

Acknowledgments

The authors acknowledge the facilities and the scientific and technical assistance of the Australian Microscopy and Microanalysis Research Facility at the Australian Centre for Microscopy and Microanalysis at the University of Sydney (Chad Moore and Ellie Kable) for the use of cell culture laboratory. We thank Nicholas Proschogo (Chemistry Mass Spectrometry Facility, the University of Sydney) for help with ESI-MS measurements.

Conflict of interest

The authors declare that the research was conducted in the absence of any commercial or financial relationships that could be construed as a potential conflict of interest.

DC declared that she was an editorial board member of Frontiers, at the time of submission. This had no impact on the peer review process and the final decision.

Generative AI statement

The author(s) declare that no Generative AI was used in the creation of this manuscript.

Publisher's note

Supplementary material

The Supplementary Material for this article can be found online at: https://www.frontiersin.org/articles/10.3389/fchbi.2025.1547323/full#supplementary-material

References

Alfieri, M. L., Cariola, A., Panzella, L., Napolitano, A., D'Ischia, M., Valgimigli, L., et al. (2022). Disentangling the puzzling regiochemistry of thiol addition to *o*-quinones. *J. Org.Chem.* 87, 4580–4589. doi:10.1021/acs.joc.1c02911

Aureliano, M., De Sousa-Coelho, A. L., Dolan, C. C., Roess, D. A., and Crans, D. C. (2023). Biological consequences of vanadium effects on formation of reactive oxygen species and lipid peroxidation. *Int. J. Mol. Sci.* 24, 5382. doi:10.3390/ijms24065382

Bates, A. C., Klugh, K. L., Galaeva, A. O., Patch, R. A., Manganaro, J. F., Markham, S. A., et al. (2025). Optimizing therapeutics for intratumoral cancer treatments: Antiproliferative vanadium complexes in glioblastoma. *Int. J. Mol. Sci.* in press. doi:10.3390/ijms26030994

Bergeron, A., Kostenkova, K., Selman, M., Murakami, H. A., Owens, E., Haribabu, N., et al. (2019). Enhancement of oncolytic virotherapy by vanadium(V) dipicolinates. *BioMetals* 32, 545–561. doi:10.1007/s10534-019-00200-9

Chen, Z., Han, F., Du, Y., Shi, H., and Zhou, W. (2023). Hypoxic microenvironment in cancer: molecular mechanisms and therapeutic interventions. *Signal Transduct. Target. Ther.* 8, 70. doi:10.1038/s41392-023-01332-8

Choroba, K., Raposo, L. R., Palion-Gazda, J., Malicka, E., Erfurt, K., Machura, B., et al. (2020). *In vitro* antiproliferative effect of vanadium complexes bearing 8-hydroxyquinoline-based ligands - the substituent effect. *Dalton Trans.* 49, 6596–6606. doi:10.1039/D0DT01017K

Cordes, E. H., and Jenks, W. P. (1962). The mechanism of Schiff-base formation and hydrolysis. *J. Am. Chem. Soc.* 84, 832–837. doi:10.1021/ja00864a031

Crans, D. C., Zhang, B., Gaidamauskas, E., Keramidas, A. D., Willsky, G. R., and Roberts, C. R. (2010) Is vanadate reduced by thiols under biological conditions? Changing the redox potential of V(V)/V(IV) by complexation in aqueous solution. *Inorg. Chem.* 49, 4245–4256. doi:10.1021/ic1000080k

Crans, D. C., Yang, L., Haase, A., and Yang, X. (2018). Health benefits of vanadium and its potential as an anticancer agent. *Metallo-Drugs Dev. Action Anticancer Agents* 18, 251–280. doi:10.1515/9783110470734-009

Dinda, R., Garribba, E., Sanna, D., Crans, D. C., and Costa Pessoa, J. (2025). Hydrolysis, ligand exchange and redox properties of vanadium compounds: implications of solution transformation on biological, therapeutic and environmental applications. *Chem. Rev.* doi:10.1021/acs.chemrev.4c00475

Erxleben, A. (2018). Transition metal salen complexes in bioinorganic and medicinal chemistry. *Inorganica Chim. Acta* 472, 40–57. doi:10.1016/j.ica.2017.06.060

Etcheverry, S. B., Ferrer, E. G., Naso, L., Rivadeneira, J., Salinas, V., and Williams, P. A. (2008). Antioxidant effects of the VO(IV) hesperidin complex and its role in cancer chemoprevention. *J. Biol. Inorg. Chem.* 13, 435–447. doi:10.1007/s00775-007-0332-9

Feng, B., Dong, Y., Shang, B., Zhang, B., Crans, D. C., and Yang, X. (2022). Convergent protein phosphatase inhibitor design for PTP1B and TCPTP: exchangeable vanadium coordination complexes on graphene quantum dots. *Adv. Funct. Mater.* 32, 2108645. doi:10.1002/adfm.202108645

Forman, H. J., Zhang, H., and Rinna, A. (2009). Glutathione: overview of its protective roles, measurement, and biosynthesis. *Mol. Aspects Med.* 30, 1–12. doi:10.1016/j.mam.2008.08.006

Freshney, R. I. (2016). *Culture of animal cells: a manual of basic technique and specialized applications*. 7th edition. Hoboken, NJ, USA: Wiley-Blackwell. ISBN: 978-1-118-87364-9.

Gao, W., Pu, L., Chen, M., Wei, J., Xin, Z., Wang, Y., et al. (2018). Glutathione homeostasis is significantly altered by quercetin via the Keap1/Nrf2 and MAPK signaling pathways in rats. *J. Clin. Biochem. Nutr.* 62, 56–62. doi:10.3164/jcbn.17-40

Gibson, D. (2009). The mechanism of action of platinum anticancer agents - what do we really know about it? *Dalton Trans.*, 10681–10689. doi:10.1039/B918871C

Griffin, E., Levina, A., and Lay, P. A. (2019). Vanadium(V) tris-3,5-di-*tert*-butylcatecholato complex: links between speciation and anti-proliferative activity in human pancreatic cancer cells. *J. Inorg. Biochem.* 201, 110815. doi:10.1016/j.jinorgbio.2019.110815

Haase, A. A., Markham, S. A., Murakami, H. A., Hagan, J., Kostenkova, K., Koehn, J. T., et al. (2024). Halogenated non-innocent vanadium(V) Schiff base complexes: chemical and anti-proliferative properties. *New J. Chem.* 48, 12893–12911. doi:10.1039/D4NJ01223B

Hall, M. D. (2022). Surrounded by ligands: the reactivity of cisplatin in cell culture medium. *J. Biol. Inorg. Chem.* 27, 691–694. doi:10.1007/s00775-022-01970-3

Hasnat, H., Shompa, S. A., Islam, M. M., Alam, S., Richi, F. T., Emon, N. U., et al. (2024). Flavonoids: a treasure house of prospective pharmacological potentials. *Heliyon* 10, e27533. doi:10.1016/j.heliyon.2024.e27533

Hepel, M., Stobiecka, M., Peachey, J., and Miller, J. (2012). Intervention of glutathione in pre-mutagenic catechol-mediated DNA damage in the presence of copper(II) ions. *Mutat. Research/Fundamental Mol. Mech. Mutagen.* 735, 1–11. doi:10.1016/j.mrfmmm.2012.05.005

Ilieva, Y., Dimitrova, L., Zaharieva, M. M., Kaleva, M., Alov, P., Tsakovska, I., et al. (2021). Cytotoxicity and microbicidal activity of commonly used organic solvents: a comparative study and application to a standardized extract from *Vaccinium Macrocarpon*. *Toxics* 9, 92. doi:10.3390/toxics9050092

Jomová, K., Hudecova, L., Lauro, P., Simunkova, M., Alwasel, S. H., Alhazza, I. M., et al. (2019). A switch between antioxidant and prooxidant properties of the phenolic compounds myricetin, morin, 3',4'-dihydroxyflavone, taxifolin and 4-hydroxy-coumarin in the presence of copper(II) ions: a spectroscopic, absorption titration and DNA damage study. *Molecules* 24, 4335. doi:10.3390/molecules24234335

Kennedy, L., Sandhu, J. K., Harper, M. E., and Cuperlovic-Culf, M. (2020). Role of glutathione in cancer: from mechanisms to therapies. *Biomolecules* 10, 1429. doi:10.3390/biom10101429

Kostenkova, K., Levina, A., Walters, D. A., Murakami, H. A., Lay, P. A., and Crans, D. C. (2023). Vanadium(V) pyridine-containing Schiff base catecholate complexes are lipophilic, redox-active and selectively cytotoxic in glioblastoma (T98G) cells. *Chem. Eur. J.* 29, e202302271. doi:10.1002/chem.202302271

Kundu, S., Maity, S., Weyhermüller, T., and Ghosh, P. (2013). Oxidovanadium catechol complexes: radical versus non-radical states and redox series. *Inorg. Chem.* 52, 7417–7430. doi:10.1021/ic400166z

Lay, P. A., and Levina, A. (1996). Kinetics and mechanism of chromium(VI) reduction to chromium(III) by L-cysteine in neutral aqueous solutions. *Inorg. Chem.* 35, 7709–7717. doi:10.1021/IC960663A

Le, M., Rathje, O., Levina, A., and Lay, P. A. (2017). High cytotoxicity of vanadium(IV) complexes with 1,10-phenanthroline and related ligands is due to decomposition in cell culture medium. *J. Biol. Inorg. Chem.* 22, 663–672. doi:10.1007/s00775-017-1453-4

León, I. E., Cadavid-Vargas, J. F., Resasco, A., Maschi, F., Ayala, M. A., Carbone, C., et al. (2016a). *In vitro* and *in vivo* antitumor effects of the VO-chrysin complex on a new three-dimensional osteosarcoma spheroids model and a xenograft tumor in mice. *J. Biol. Inorg. Chem.* 21, 1009–1020. doi:10.1007/s00775-016-1397-0

León, I. E., Díez, P., Etcheverry, S. B., and Fuentes, M. (2016b). Deciphering the effect of an oxovanadium(IV) complex with the flavonoid chrysin (VOChrys) on intracellular cell signalling pathways in an osteosarcoma cell line. *Metallomics* 8, 739–749. doi:10.1039/c6mt00045b

Levina, A., Crans, D. C., and Lay, P. A. (2017). Speciation of metal drugs, supplements and toxins in media and bodily fluids controls *in vitro* activities. *Coord. Chem. Rev.* 352, 473–498. doi:10.1016/j.ccr.2017.01.002

Levina, A., Crans, D. C., and Lay, P. A. (2022). Advantageous reactivity of unstable metal complexes: potential applications of metal-based anticancer drugs for intratumoral injections. *Pharmaceutics* 14, 790. doi:10.3390/pharmaceutics14040790

Levina, A., and Lay, P. A. (2017). Stabilities and biological activities of vanadium drugs: what is the nature of the active species? *Chem. – Asian J.* 12, 1692–1699. doi:10.1002/asia.201700463

Levina, A., and Lay, P. A. (2020). Vanadium(V/IV) - transferrin binding disrupts the transferrin cycle and reduces vanadium uptake and antiproliferative activity in human lung cancer cells. *Inorg. Chem.* 59, 16143–16153. doi:10.1021/acs.inorgchem.0c00926

Levina, A., Pires Vieira, A., Wijetunga, A., Kaur, R., Koehn, J. T., Crans, D. C., et al. (2020). A short-lived but highly cytotoxic vanadium(V) complex as a potential drug lead for brain cancer treatment by intratumoral injections. *Angew. Chem. Int. Ed.* 59, 15834–15838. doi:10.1002/anie.202005458

Levina, A., Scalese, G., Gambino, D., Crans, D. C., and Lay, P. A. (2024). Solution chemistry and anti-proliferative activity against glioblastoma cells of a vanadium(V) complex with two bioactive ligands. *Front. Chem. Biol.* 3, 1394645. doi:10.3389/fchbi.2024.1394645

Levina, A., Uslan, C., Murakami, H., Crans, D. C., and Lay, P. A. (2023). Substitution kinetics, albumin and transferrin affinities, and hypoxia all affect the biological activities of anticancer vanadium(V) complexes. *Inorg. Chem.* 62, 17804–17817. doi:10.1021/acs.inorgchem.3c02561

Li, C., Zhang, W. J., Choi, J., and Frei, B. (2016). Quercetin affects glutathione levels and redox ratio in human aortic endothelial cells not through oxidation but formation and cellular export of quercetin-glutathione conjugates and upregulation of glutamate-cysteine ligase. *Redox Biol.* 9, 220–228. doi:10.1016/j.redox.2016.08.012

Lima, L. M. A., Murakami, H., Gaebler, D. J., Silva, W. E., Belian, M. F., Lira, E. C., et al. (2021). Acute toxicity evaluation of non-innocent oxidovanadium(V) Schiff base complex. *Inorganics* 9, 42. doi:10.3390/inorganics9060042

Liu, Z., Huang, T., Shi, Q., Deng, Z., and Lin, S. (2023). Catechol siderophores framed on 2,3-dihydroxybenzoyl-L-serine from *Streptomyces varsoviensis*. *Front. Microbiol.* 14, 1182449. doi:10.3389/fmicb.2023.1182449

Lyu, Q., Hsueh, N., and Chai, C. L. L. (2019). The chemistry of bioinspired catechol(amine)-based coatings. *ACS Biomater. Sci. Eng.* 5, 2708–2724. doi:10.1021/acsbiomaterials.9b00281

McAusland, T. M., Van Vloten, J. P., Santry, L. A., Guilleman, M. M., Rghei, A. D., Ferreira, E. M., et al. (2021). Combining vanadyl sulfate with Newcastle disease virus potentiates rapid innate immune-mediated regression with curative potential in murine cancer models. *Mol. Ther. - Oncolytics* 20, 306–324. doi:10.1016/j.omto.2021.01.009

McLauchlan, C. C., Peters, B. J., Willsky, G. R., and Crans, D. C. (2015). Vanadium–phosphatase complexes: phosphatase inhibitors favor the trigonal bipyramidal transition state geometries. *Coord. Chem. Rev.* 301-302, 163–199. doi:10.1016/j.ccr.2014.12.012

Murakami, H. A., Uslan, C., Haase, A. A., Koehn, J. T., Vieira, A. P., Gaebler, D. J., et al. (2022). Vanadium chloro-substituted Schiff base catecholate complexes are reducible, lipophilic, water stable, and have anticancer activities. *Inorg. Chem.* 61, 20757–20773. doi:10.1021/acs.inorgchem.2c02557

Naso, L. G., Ferrer, E. G., and Williams, P. A. M. (2023). Correlation of the anticancer and pro-oxidant behavior and the structure of flavonoid-oxidovanadium(IV) complexes. *Coord. Chem. Rev.* 492, 215271. doi:10.1016/j.ccr.2023.215271

Nunes, P., Correia, I., Cavaco, I., Marques, F., Pinheiro, T., Avecilla, F., et al. (2021). Therapeutic potential of vanadium complexes with 1,10-phenanthroline ligands, *quo vadis*? Fate of complexes in cell media and cancer cells. *J. Inorg. Biochem.* 217, 111350. doi:10.1016/j.jinorgbio.2020.111350

Nunes, P., Correia, I., Marques, F., Matos, A. P., Dos Santos, M. M. C., Azevedo, C. G., et al. (2020). Copper complexes with 1,10-phenanthroline derivatives: underlying factors affecting their cytotoxicity. *Inorg. Chem.* 59, 9116–9134. doi:10.1021/acs.inorgchem.0c00925

Pavlíková, N. (2022). Caffeic acid and diseases-mechanisms of action. *Int. J. Mol. Sci.* 24, 588. doi:10.3390/ijms24010588

Pereira, M. R. G., Oliveira, E. S. D., Villar, F. A. G. A. D., Grangeiro, M. S., Fonseca, J., Silva, A. R. D., et al. (2004). Cytotoxicity of catechol towards human glioblastoma cells via superoxide and reactive quinones generation. *J. Bras. Patol. Med. Lab.* 40, 280–285. doi:10.1590/s1676-24442004000400012

Pessoa, J. C., and Correia, I. (2019). Salan vs. salen metal complexes in catalysis and medicinal applications: virtues and pitfalls. *Coord. Chem. Rev.* 388, 227–247. doi:10.1016/j.ccr.2019.02.035

Pessoa, J. C., Etcheverry, S., and Gambino, D. (2015). Vanadium compounds in medicine. *Coord. Chem. Rev.* 301-302, 24–48. doi:10.1016/j.ccr.2014.12.002

Pierpont, C. G. (2001). Studies on charge distribution and valence tautomerism in transition metal complexes of catecholate and semiquinonate ligands. *Coord. Chem. Rev.* 216-217, 99–125. doi:10.1016/s0010-8545(01)00309-5

Rajashekar, C. B. (2023). Dual role of plant phenolic compounds as antioxidants and prooxidants. *Am. J. Plant Sci.* 14, 15–28. doi:10.4236/ajps.2023.141002

Reytman, L., Hochman, J., and Tshuva, E. Y. (2018). Anticancer diaminotris(phenolato) vanadium(V) complexes: ligand-metal interplay. *J. Coord. Chem.* 71, 2003–2011. doi:10.1080/00958972.2018.1461848

Ścibior, A. (2022). Overview of research on vanadium-quercetin complexes with a historical outline. *Antioxidants* 11, 790. doi:10.3390/antiox11040790

Selman, M., Rousso, C., Bergeron, A., Son, H. H., Krishnan, R., El-Sayes, N. A., et al. (2018). Multi-modal potentiation of oncolytic virotherapy by vanadium compounds. *Mol. Ther.* 26, 56–69. doi:10.1016/j.ymthe.2017.10.014

Selvaraj, S., and Krishnan, U. M. (2021). Vanadium-flavonoid complexes: a promising class of molecules for therapeutic applications. *J. Med. Chem.* 64, 12435–12452. doi:10.1021/acs.jmedchem.1c00405

Shukla, R., Barve, V., Padhye, S., and Bhonde, R. (2006). Reduction of oxidative stress induced vanadium toxicity by complexing with a flavonoid, quercetin: a pragmatic therapeutic approach for diabetes. *Biometals* 19, 685–693. doi:10.1007/s10534-006-9005-3

Someya, Y., Saito, S., Takeda, S., Adachi, N., and Kurosawa, A. (2024). Quercetin exhibits cytotoxicity in cancer cells by inducing two-ended DNA double-strand breaks. *Biochem. Biophysical Res. Commun.* 739, 150977. doi:10.1016/j.bbrc.2024.150977

Stone, A. T., Dhara, V. G., Naik, H. M., Aliyu, L., Lai, J., Jenkins, J., et al. (2021). Chemical speciation of trace metals in mammalian cell culture media: looking under the hood to boost cellular performance and product quality. *Curr. Opin. Biotechnol.* 71, 216–224. doi:10.1016/j.copbio.2021.08.004

Sylvester, P. W. (2011). Optimization of the tetrazolium dye (MTT) colorimetric assay for cellular growth and viability. *Methods Mol. Biol.* 716, 157–168. doi:10.1007/978-1-61779-012-6_9

Tadele, K. T., and Tsega, T. W. (2019). Schiff bases and their metal complexes as potential anticancer candidates: a review of recent works. *Anti-Cancer Agents Med. Chem.* 19, 1786–1795. doi:10.2174/1871520619666190227171716

Turell, L., Radi, R., and Alvarez, B. (2013). The thiol pool in human plasma: the central contribution of albumin to redox processes. *Free Radic. Biol. Med.* 65, 244–253. doi:10.1016/j.freeradbiomed.2013.05.050

van Bergeijk, D. A., Elsayed, S. S., Du, C., Santiago, I. N., Roseboom, A. M., Zhang, L., et al. (2022). The ubiquitous catechol moiety elicits siderophore and angucycline production in Streptomyces. *Commun. Chem.* 5, 14. doi:10.1038/s42004-022-00632-4

Walencik, P. K., Choińska, R., Gołębiewska, E., and Kalinowska, M. (2024). Metal-flavonoid interactions - from simple complexes to advanced systems. *Molecules* 29, 2573. doi:10.3390/molecules29112573

Xu, D., Hu, M. J., Wang, Y. Q., and Cui, Y. L. (2019). Antioxidant activities of quercetin and its complexes for medicinal application. *Molecules* 24, 1123. doi:10.3390/molecules24061123

Xu, S., Liu, H., Li, X., Zhao, J., Wang, J., Crans, D. C., et al. (2024). Approaches to selective and potent inhibition of glioblastoma by vanadyl complexes: inducing mitotic catastrophe and methuosis. *J. Inorg. Biochem.* 257, 112610. doi:10.1016/j.jinorgbio.2024.112610

Yin, C.-X., and Finke, R. G. (2005a). Kinetic and mechanistic studies of vanadium-based, extended catalytic lifetime catechol dioxygenases. *J. Am. Chem. Soc.* 127, 13988–13996. doi:10.1021/ja052998+

Yin, C.-X., and Finke, R. G. (2005b). Vanadium-based, extended catalytic lifetime catechol dioxygenases: evidence for a common catalyst. *J. Am. Chem. Soc.* 127, 9003–9013. doi:10.1021/ja051594e